Analysis of band-gap formation in squashed armchair carbon nanotubes

H. Mehrez, A. Svizhenko, and M. P. Anantram
Mail Stop: 229-1, Center for NanoTechnology and NASA Advanced Supercomputing Division, NASA Ames Research Center, Moffett Field, California 94035-1000, USA

M. Elstner and T. Frauenheim
Theoretische Physik, Universitat Paderborn, D-33098 Paderborn, Germany
(Received 6 December 2004; published 28 April 2005)

The electronic properties of deformed armchair carbon nanotubes are modeled using constraint free density functional tight binding molecular dynamics simulations. Independent from CNT diameter, deforming path can be divided into *three* regimes. In the first regime, the nanotube deforms with negligible force. In the second one, there is significantly more resistance to deforming with the force being ~40–100 nN/per CNT unit cell. In the last regime, the CNT loses its hexagonal structure resulting in force drop-off followed by substantial force enhancement upon deforming. We compute the change in band gap as a function of deforming and our main results are: (i) A band gap initially opens due to interaction between atoms at the top and bottom sides of CNT. The π-orbital approximation is successful in modeling the band-gap opening at this stage. (ii) In the second regime of deforming, large π-σ interaction at the edges becomes important, which can lead to band-gap oscillation. (iii) Contrary to a common perception, nanotubes with broken mirror symmetry can have *zero* band gap. (iv) All armchair nanotubes become metallic in the third regime of deforming. Finally, we discuss both differences and similarities obtained from the tight binding and density functional approaches.

DOI: 10.1103/PhysRevB.71.155421 PACS number(s): 73.63.Fg, 61.46.+w, 73.22.−f

I. INTRODUCTION

Experiments probing the electromechanical response of carbon nanotubes have been the most interesting recent work in nanotubes.[1–5] These experiments involve nanotubes interacting electrically with contacts and mechanically with an atomic force microscope (AFM) tip. Apart from the fundamental physics governing the electromechanical response, these experiments are also important for future use of carbon nanotubes as actuators and nano electromechanical devices.[6] There are two categories of experiments exploring the electromechanical properties. The first category involves deformation of a suspended nanotube with an AFM tip.[3–5] The electrical conductance was found to decrease by two orders of magnitude upon modest deformation due to bond stretching which results in band-gap opening at Fermi energy.[7] The second category of experiments involves the deforming of nanotubes lying on a hard substrate.[1,2] In the experiment of Gomez *et al.*[2] a metal to semiconductor transition has been demonstrated in a deformed metallic nanotube. Theoretically, there have been several studies that modeled the electromechanical properties of deformed carbon nanotubes.[8–11] It was found that mirror symmetry breaking and formation of bonds between atoms at the top-bottom sides of CNT are necessary to open a band gap in an armchair nanotube. While Refs. 9 and 10 performed energy relaxation by enforcing specific symmetries during deformation, Ref. 11 modeled deforming by a tip whose width was 5.8 Å, which is smaller than even a (6,6) nanotube diameter.

In this study, we model the tip-nanotube interaction more realistically by performing constraint free density functional tight binding (DF-TB) molecular dynamics (MD) simulations. Our calculations differ from prior work in that we do not impose specific symmetry conditions and allow for the nanotube to change symmetry during deformation. Further, our tip diameter is larger than the nanotube diameter, as in the experiments of Refs. 1 and 2. The aim of our work is to investigate: (i) the magnitude of the force required to deform CNT, (ii) dependence of band-gap formation on the initial conditions of the MD simulations, (iii) applicability of π-orbital theories to find the band-gap upon deformation, (iv) relative roles of interactions between atoms at the top-bottom sides and atoms at the edges on the band-gap, (v) the electronic properties of a CNT deformed beyond the reversible regime, (vi) diameter dependence on the band-gap opening upon deforming, and (vii) effect of self-consistent calculations on band-gap formation.

We will address the aforementioned issues in the rest of the paper. Initially we describe our method to simulate the experiment. Following this we present the mechanical properties of deformed CNT in Sec. III. In Sec. IV, various aspects on the electronic properties of deformed CNT will be investigated. Finally, the conclusion will be given in Sec. V.

II. METHODOLOGY

A (n,n) CNT is generated from a planar rolled graphene strip, where $n \in \{6,7,8,9,10,11,12\}$. The corresponding diameters of these CNTs are in the range of ~8–16 Å. If such tubes are deformed in an AFM set-up, the tip radius is at least *one order* of magnitude larger than the CNT diameter. Hence we approximate the tip as a rigid graphene sheet where the atoms do not relax. The substrate is also modeled as a rigid graphene sheet. The distance between the graphene sheets and CNT edges is at least 4.5 Å at the beginning of the MD simulations, so that CNT is not deformed in the first step. A snapshot of the atomic configuration of a deformed

 ©2005 The American Physical Society

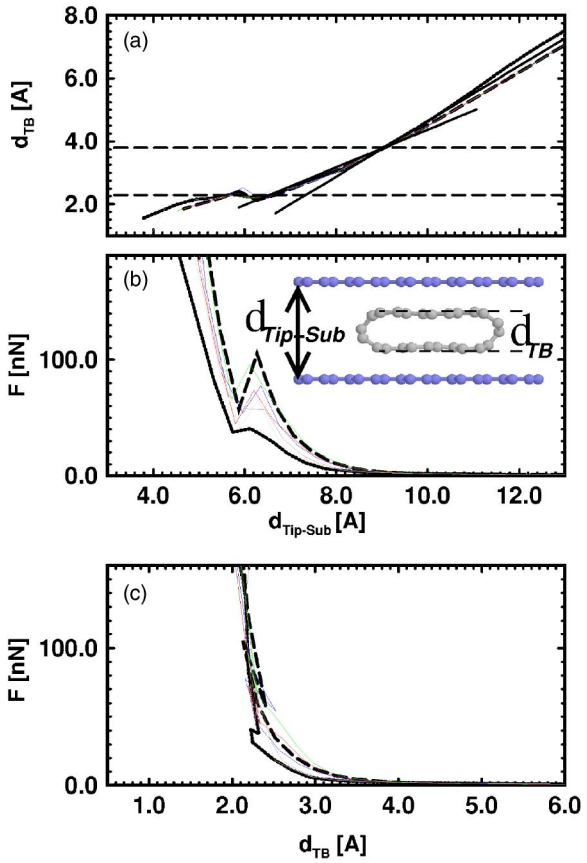


FIG. 1. (Color online) The inset in (b) displays the atomic configuration of a deformed CNT between tip and sample. $d_{\text{Tip-Sub}}$, and d_{TB} are the tip-sample separation distance and the distance between top and bottom sides of CNT, respectively. (a) d_{TB} vs $d_{\text{Tip-Sub}}$; CNT deforming undergoes *three* regimes, $d_{\text{TB}} > 3.8$ Å, 3.8 Å $> d_{\text{TB}} > 2.3$ Å, and $d_{\text{TB}} < 2.3$ Å. These regimes are separated by the horizontal dashed lines. In the first regime, the slope of d_{TB} vs $d_{\text{Tip-Sub}}$ is $\sim 0.88 \pm 0.07$ while in the second regime the slope is $\sim 0.6 \pm 0.05$, where the corresponding fits are represented as thick solid lines. At $d_{\text{TB}} < 2.3$ Å, CNT undergoes structural transformation and the honeycomb structure cannot be identified. (b),(c) Force exerted on the tip (top graphene sheet) as a function of $d_{\text{Tip-Sub}}$ and d_{TB}, respectively. In all panels, every thin line corresponds to one simulation and results for (6,6) and (12,12) CNT are highlighted as thick dotted lines and dashed lines, respectively.

CNT between tip and sample is shown in the inset of Fig. 1(b). To model deforming of CNT we adopt two different methods: the first method consists of moving both the tip and substrate symmetrically towards the nanotube and the second one consists of moving only the tip towards the nanotube. We do not employ any further constraint on CNT atoms.

The MD simulations are performed using DFTB, which is a density functional theory based tight binding approach.[12,13] At each MD step of deforming, forces are calculated using the Hellmann-Feynman[14,15] theorem and CNT atoms are fully relaxed by the conjugate gradient method. Convergence criteria on the relaxed CNT structure is set such that the maximum force on each CNT atom is $<10^{-4}$ a.u. We have deformed the nanotubes all the way to the irreversible regime. That is, the CNT structure is lost at the end of the simulation and cannot be recovered if the graphene sheets are removed. Since CNTs are constraint free, both "tank treading" (motion of atoms along circumference) and translational motion at various stages of deforming are possible if the energetics is favorable to such movement. We have also found that the symmetry of deformed CNT depends on the initial conformation of the CNT with respect to tip and substrate as well as the method adopted to deform CNT.

As CNT is being deformed, atoms follow various trajectories depending on the details of initial and ambient conditions. This would affect the conformation of the CNT with respect to the AFM tip as well as the symmetry of the CNT itself during deforming. To model this experiment faithfully and to draw more general conclusions on the electromechanical properties of deformed armchair CNTs, various simulations are required. In our work, constraint free deforming of more than *fifteen* paths have been performed on various CNTs and this represents substantial improvement over previous simulations.[9–11]

III. MECHANICAL PROPERTIES

Our MD simulations reveal *three* different regimes of a deformed nanotube. These regimes can be clearly resolved by plotting the distance between top and bottom sides of the nanotube (d_{TB}) vs tip-substrate separation distance ($d_{\text{Tip-Sub}}$) as shown in Fig. 1(a) as well as the force on the tip vs $d_{\text{Tip-Sub}}$ as shown in Fig. 1(b). In the first regime, d_{TB} is larger than 3.8 Å and the nanotube is compressed relatively easily. This is reflected in the rather large slope $\Delta d_{\text{TB}}/\Delta d_{\text{Tip-Sub}} \sim 0.88 \pm 0.07$ as seen in Fig. 1(a), and small force of less than 10 nN/per CNT unit cell on the tip as seen in Fig. 1(b). The second regime of deforming corresponds to $d_{\text{TB}} \sim 2.3$–3.8 Å. Here the nanotube is more rigid to compression as seen by the moderate value of $\Delta d_{\text{TB}}/\Delta d_{\text{Tip-Sub}} \sim 0.6 \pm 0.05$, and the relatively large value of force on the tip, 40–100 nN/per CNT unit cell. These two regimes are reversible, i.e., retracting the tip and substrate results in a reversible change of the nanotube. The third regime corresponds to $d_{\text{TB}} < 2.3$ Å and is characterized by an irreversible change, where the honeycomb structure of the nanotube is lost. The nanotube undergoes major atomic rearrangements so that total energy of the system is reduced. The CNT structural relaxation is also accompanied by force drop-off on the tip. However, this is substantially enhanced upon further deforming as seen in Fig. 1(b). An interesting feature of this regime is that atoms at the top and bottom sides of the CNT are no longer planar. They form a sawtooth structure and results in an increase of d_{TB} with a decrease in $d_{\text{Tip-Sub}}$ as shown in Fig. 1(a).

In Figs. 1(b) and 1(c) we present the force curves on the tip for all CNTs as a function of $d_{\text{Tip-Sub}}$ and d_{TB} respectively. The curves corresponding to (6,6) and (12,12) nanotubes are shown as thick dotted and dashed lines, respectively. Comparison of the two curves indicates that, in general the force on the tip increases with increase in the nanotube diameter. However, we find that the force required to deform an (11,11) nanotube (shown as thin lines) is larger than the one needed for a (12,12) nanotube when $d_{\text{TB}} > 2.3$ Å. The under-

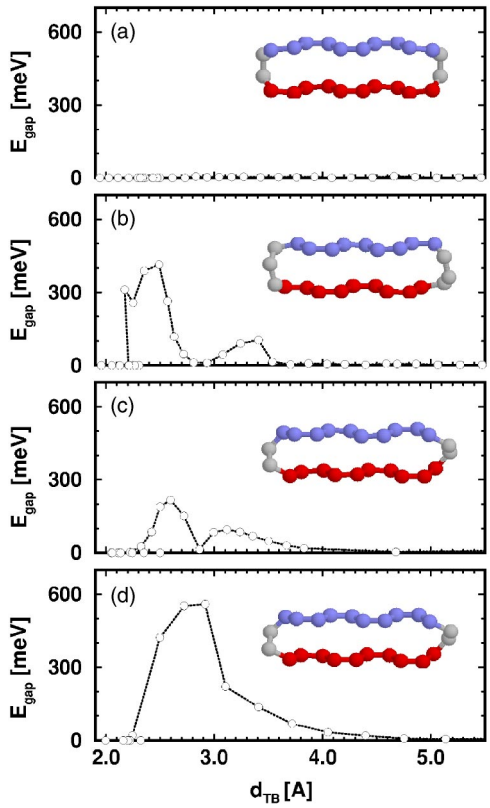


FIG. 2. (Color online) E_g of (6,6) CNT at E_F as a function of d_{TB} for different simulations. In (a) and (b) only the top graphene layer is displaced, while in (c) and (d) both layers are moved to deform CNT. The insets in each panel show the atomic configuration of the corresponding CNT unit cell for d_{TB} 2.90±0.05 Å where gray atoms and dark gray atoms indicate top and bottom sides of CNT, respectively.

lying reason for this discrepancy is that the mirror symmetry is preserved during this simulation of the (11,11) nanotube while broken in the (12,12) CNT. If the nanotube mirror symmetry is preserved, atoms at the top-bottom sides of the nanotube are aligned. This results in a "more robust" structure, which offers resistance to deforming. Overall, our results indicate that the force required to deform nanotubes increases with an increase in diameter, and is larger for conformation which preserves mirror symmetry.

IV. ELECTRONIC PROPERTIES

(6,6) arm-chair CNT has been investigated substantially and we start our discussion on the electronic properties of this tube. Depending on the initial orientation of the tube with respect to the graphene sheets and the manner of deforming, structural deformation may proceed along different paths. At each step of these paths and when the CNT atoms are fully relaxed, we compute the band structure and find the band gap. Figure 2 shows an evolution of the band gap as a function of d_{TB} for different paths. Qualitatively, one can see common features corresponding to the three regimes of deforming.

In the first regime, when $d_{\mathrm{TB}} > 3.8$ Å, initially metallic (6,6) CNT shows a zero band gap. The transition to the second regime is manifested by the opening of the band gap at $d_{\mathrm{TB}} \sim 3.8$ Å [Figs. 2(b)–2(d)]. It is at this deformation that atoms at the top and bottom sides of the CNT start to interact, which leads to the stiffening of the tube and to the modification of the band structure. The interaction between top and bottom sides of the CNT induces a perturbation term to ideal CNT Hamiltonian $\mathbf{H}_0$. We define this additional term as $\Delta\mathbf{H}_{\mathrm{TB}}$ and it corresponds to the interaction between atoms shown as gray and dark gray (or light blue and red) atoms in the insets of each panel of Fig. 2. We note, that the opening of the band gap may occur only when the mirror symmetry of the tube is broken, which is not the case in Fig. 2(a).

In the second regime, where CNT is deformed such that 2.3 Å $< d_{\mathrm{TB}} <$ 3.8 Å, major changes to the band gap occur. The most striking feature is that while the band structure is qualitatively similar to that of the undeformed nanotube, *the band gap oscillates*, becoming *zero*, as in Figs. 2(b) and 2(c), at $d_{\mathrm{TB}} \sim 2.90$ Å. Another important observation is that the symmetry of the tube is constantly changing in the course of deformation. Sudden changes of symmetry are accompanied by steep changes of band gap, as in Fig. 2(d) at $d_{\mathrm{TB}} \sim 3.0$ Å. The galore of various scenarios of band-gap behavior under deforming raises a question about the robustness and universality of the conductance modulation in such experiments. There are two sources of uncertainty. The first one is the constantly changing symmetry of the tube which leads to an "on-off" behavior of conductance as discussed in Sec. IV A. The second one is due to a collective effect of top-bottom and edge atomic interactions. As will be shown in Sec. IV B, the curvature at the edges induces large π-σ interactions, which may enhance or cancel the band gap due to π-π^* interactions between top and bottom atoms. This edge interaction, $\Delta\mathbf{H}_{\mathrm{ED}}$, is defined such that the deformed CNT Hamiltonian is $\mathbf{H}_s = \mathbf{H}_0 + \Delta\mathbf{H}_{\mathrm{TB}} + \Delta\mathbf{H}_{\mathrm{ED}}$. In this regime $\Delta\mathbf{H}_{\mathrm{ED}}$ induces the π-σ interaction and the band gap cannot be deduced within the π-orbital model.

Finally, in the third regime, where $d_{\mathrm{TB}} < 2.3$ Å, we find that the band gap vanishes in all the simulations. At this stage the CNT undergoes irreversible structural transformation where the honeycomb geometry is lost. The electronic band structure of a completely deformed nanotube resembles that of a metal, with multiple subbands passing through E_F. Previous studies[11] predicted that the nanotube will always become semiconducting in the course of deforming due to a spontaneous symmetry breaking. However, we find that it is possible for a structure to remain mirror symmetrical all the way till the irreversible regime as in the case of Fig. 2(a). Although mirror symmetry is broken in the irreversible regime, this does not lead to the band-gap opening.

A. The role of symmetry breaking in the formation of the band gap

One can understand the band-gap opening in the first regime within a simple model.[11] In this model only a single π-orbital/atom is taken into account. In addition to this, deforming is treated as a *first* order degenerate perturbation of the crossing subbands, π and π^* of an ideal armchair CNT. At the crossing point, the energy eigenstates are determined

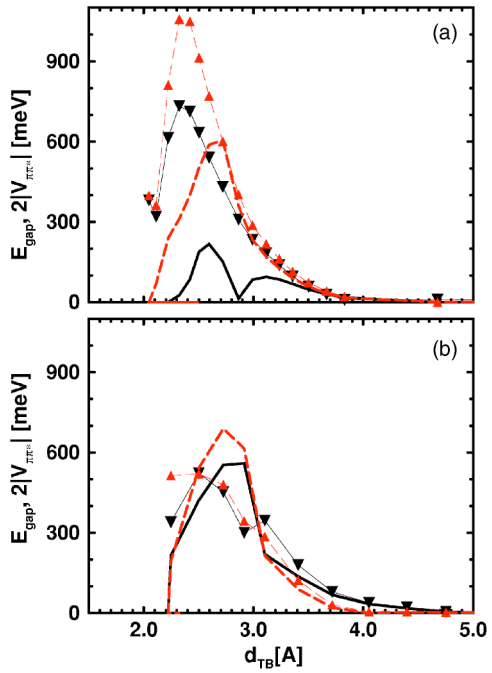


FIG. 3. (Color online) (a) and (b) show the band gap at E_F and $2|V_{\pi\pi^*}|$ of (6,6) CNT for simulation results shown in Figs. 2(c) and 2(d); respectively. Continuous lines and dashed lines correspond to E_g using 4 orbitals/atom and a single π-orbital/atom, respectively. Thin lines with triangle down symbols and dashed lines with triangle-up symbols represent $2|V_{\pi\pi^*}|$ using 4 orbitals/atom and a single π-orbital/atom, respectively.

by diagonalizing the perturbation Hamiltonian,[11]

$$\mathbf{H}^p = \begin{pmatrix} V_{\pi\pi} & V_{\pi\pi^*} \\ V_{\pi^*\pi} & V_{\pi^*\pi^*} \end{pmatrix} \quad (1)$$

where $\mathbf{H}^p = \mathbf{H}_s - \mathbf{H}_0$ and $\mathbf{H}_s, \mathbf{H}_0$ are the Hamiltonians of deformed and ideal CNTs, respectively. The diagonal term in Eq. (1) results in an energy shift of π and π^* bands by $V_{\pi\pi}$ and $V_{\pi^*\pi^*}$, respectively. This shifts the subbands crossing point but does not lead to a bandgap. If the off-diagonal term is applied a band gap E_g opens at Fermi energy E_F, such that $E_g = 2|V_{\pi\pi^*}|$.

In Fig. 3(a) and 3(b) we show that this approximation describes well the band-gap opening in the first regime ($d_{TB} > 3.8$ Å) for results presented in Figs. 2(c) and 2(d). However, at slightly higher deformations both the π-orbital representation and the perturbation approach fail, as elaborated in the next subsection.

A band-gap opening in armchair nanotubes has been correlated to the mirror symmetry breaking;[9–11] when the mirror symmetry is broken and bonds between top and bottom atoms are formed, $V_{\pi\pi^*}$ becomes non*zero* and the band gap opens up. The underlying mechanism is to make the two originally equivalent sublattices **A** and **B** of the CNT distinguishable.[16] To investigate the rigor of the correlation between the band gap and mirror symmetry breaking, we have analyzed CNT atomic positions as a function of deforming. In each panel of Fig. 2 we display a snapshot of *one* (6,6) CNT ring at $d_{TB} = 2.90 \pm 0.05$ Å. It is clear from Fig. 2(a), that mirror symmetry is preserved and indeed the band gap does not develop in the course of deforming. However, mirror symmetry is broken for the other simulations as indicated by the rest of the insets of Fig. 2. Yet, our calculations, which include 4-orbitals/atom, show that the band gap vanishes at $d_{TB} \sim 2.9$ Å for panels (b) and (c) of Fig. 2. These results indicate clearly that the degree to which sublattices **A** and **B** are distinguishable is not the main factor in determining the magnitude of the band gap upon deformation. We conclude that *mirror symmetry breaking is necessary, but not sufficient for the band-gap opening*, and thus can not be used as a general guide to the metal-to-semiconductor transition.

B. Failure of π-orbital representation and perturbation approach

We now check the validity of the above model for the description of the band gap. The sp^3 (4 orbitals/atom) representation of a CNT Hamiltonian ($\mathbf{H}_0$ or $\mathbf{H}_s$) can be transformed into *two* subblocks $\mathbf{H}_{sp2}$ and $\mathbf{H}_\pi$.[17] The band structure of an undeformed carbon nanotube in the vicinity of the Fermi energy E_F, can be described using only the π-orbital Hamiltonian, $\mathbf{H}_\pi$. The band gap derived using the single π-orbital/atom model for these systems is shown in Figs. 3(a) and 3(b) as dashed lines. It is clear from Fig. 3(a) that, for $d_{TB} < 3.5$ Å, the single π-orbital/atom model overestimates the band gap and does not predict the dip at $d_{TB} \sim 2.9$ Å. Similarly, it fails to determine band gap E_g for $d_{TB} < 4.5$ Å in Fig. 3(b). These results show that the band structure is determined by interactions between all orbitals, rather than π-orbitals alone.

We have also tested the rigor of perturbation theory, i.e., whether the band gap E_g can be estimated as $2|V_{\pi\pi^*}|$. In Fig. 3, we display the value of $2|V_{\pi\pi^*}|$ calculated using the full Hamiltonian (triangle down symbols) and the π-orbital Hamiltonian (triangle up). It is clear that within sp^3 model perturbation theory results do not match E_g for $d_{TB} < 3.5$ (3.7) Å in Fig. 3(a) and 3(b). Even if a single π-orbital/atom model is employed, perturbation theory results fail to describe E_g for $d_{TB} < 2.8$ (3.0) Å in Fig. 3(a) and 3(b). Hence we conclude that neither the single π-orbital/atom model nor perturbation theory, assumed in Eq. (1) is able to describe the electronic band structure of a deformed armchair carbon nanotube.

To determine the origin of single π-orbital/atom failure to describe the electronic properties of deformed armchair CNT in the vicinity of E_F, we decompose the perturbation Hamiltonian, $\mathbf{H}_s - \mathbf{H}_0$, to a sum of top-bottom and edge interaction, $\Delta\mathbf{H}_{TB}$ and $\Delta\mathbf{H}_{ED}$. We define $\mathbf{H}_{TB} = \mathbf{H}_0 + \Delta\mathbf{H}_{TB}$ and use this Hamiltonian to find the band gap, shown in Figs. 4(a) and 4(b), for the structures discussed in Fig. 3(a) and 3(b). We note that single π-orbital/atom model describes E_g due to all top-bottom interaction Hamiltonian accurately. Moreover, this band gap can be modeled within perturbation theory between π and π^* states for $d_{TB} \geq 2.7$ Å. If CNT is deformed such that $d_{TB} \leq 2.7$ Å, top-bottom interaction is substantially enhanced and perturbation theory fails to predict the band gap.

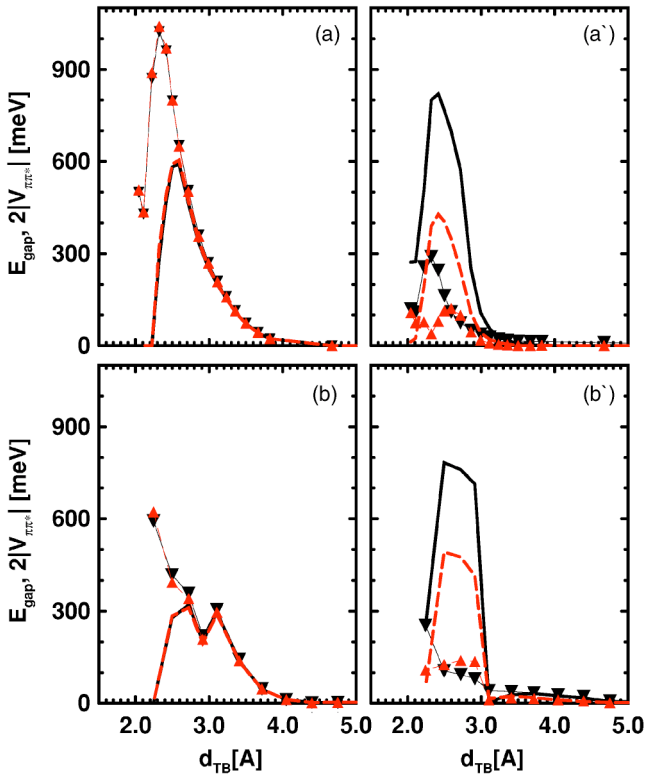


FIG. 4. (Color online) (a),(b) and (a′),(b′) show the band gap at E_F and $2|V_{\pi\pi^*}|$ of (6,6) CNT for simulation results shown in Figs. 2(c) and 2(d) due to top-bottom interactions ($\mathbf{H}_{\mathrm{TB}}$) and edge effects ($\mathbf{H}_{\mathrm{ED}}$), respectively. Top and bottom of CNT are shown in the insets of Fig. 2 with gray and dark gray atoms. In these panels, continuous and dashed lines correspond to E_g using 4 orbitals/atom and a single π-orbital/atom, respectively. Thin lines with triangle down symbols and dashed lines with triangle-up symbols represent $2|V_{\pi\pi^*}|$ using 4 orbitals/atom and a single π-orbital/atom, respectively.

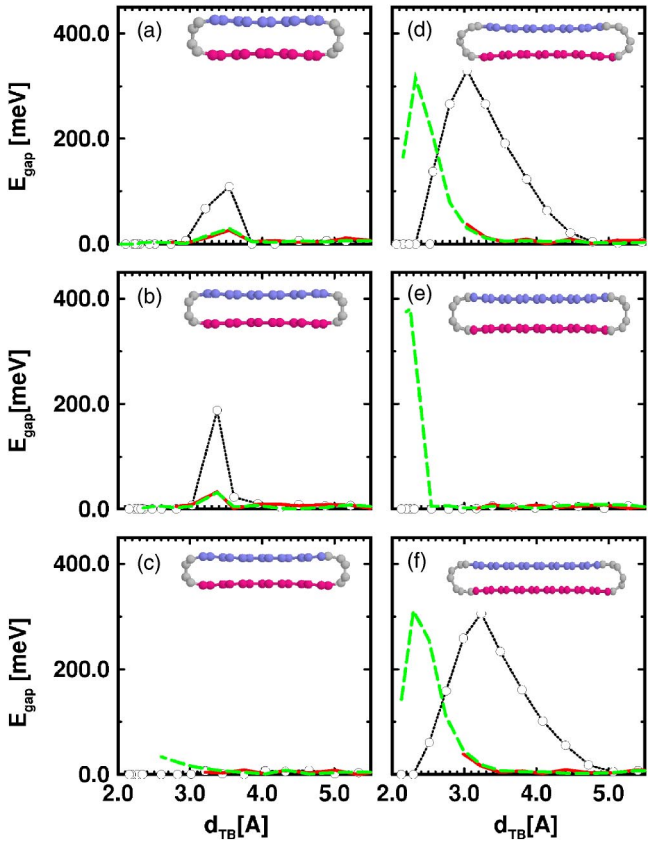


FIG. 5. (Color online) Band gap of armchair CNTs as a function of deforming. (a), (b), (c), (d), (e), and (f) correspond to (7,7), (8,8), (9,9), (10,10), (11,11), and (12,12) tubes, respectively. Dotted lines with open circles correspond to all interactions, continuous lines are interactions up-to the *second* nearest neighbor and dashed lines correspond to results when top-bottom interactions are omitted. The insets in each panel show the atomic configuration of the corresponding CNT unit cell for d_{TB} closest to 3.2 Å where top and bottom sides of CNT are highlighted.

When similar analysis is applied to the interactions at the edges, $\mathbf{H}_{\mathrm{ED}}=\mathbf{H}_0+\Delta\mathbf{H}_{\mathrm{ED}}$, we find that the single π-orbital/atom model as well as perturbation theory fail to reproduce full model calculations, as shown in Figs. 4(a′) and 4(b′). We see that a single π-orbital/atom model underestimates the true band gap E_g computed using 4 orbitals/atom, while the perturbation theory result $2|V_{\pi\pi^*}|$ predicts a much smaller value. These graphs indicate that at the high curvature edge regions, π-σ interaction is large compared to π-π^* interaction and cannot be neglected.

The degree of sophistication required to describe the band gap of a deformed CNT in the second regime can be summarized by the following steps: (i) if the mirror symmetry is broken, top bottom interaction induces a band-gap opening, which can be predicted within the single π-orbital/atom model and a perturbation theory; (ii) Further deforming increases π-σ interaction at the edges due to large curvature. This interaction necessitates the use of full calculation within sp^3 model. It is also important to note that neither top-bottom nor edge interactions alone can explain the dips of the band gap. Only cancellation effect of both interactions leads to the oscillations of the band gap in Figs. 2(b) and 2(c).

C. Effect of CNT diameter

In this subsection we highlight the most important results for arm-chair CNTs with larger diameters. In Fig. 5 we show the band gap of (n,n) nanotubes as a function of deforming, where $n\in\{7,8,9,10,11,12\}$.

In each panel of Fig. 5, we display a snapshot of the atomic configuration of the corresponding CNT. These insets indicate that when mirror symmetry is strongly broken, a larger band gap is formed. The origin of this gap is of the same nature as in the (6,6) CNT. It is due to top-bottom interactions as well as edge effects. In Fig. 5, we present the gap results when including only interactions up to *second* nearest neighbor as continuous lines while dashed lines include full Hamiltonian except top-bottom interactions. We note that the Hamiltonian which takes into account only *first* and *second* nearest neighbors is similar to edge interaction Hamiltonian $\mathbf{H}_{\mathrm{ED}}$. These results indicate that edge effect on the band gap formation is relevant only for $d_{\mathrm{TB}}\leqslant 3.5$ Å. The initiation of the gap at large separation distance, d_{TB}, is solely due to top-bottom interactions as found for (6,6) CNTs.

Our simulations also show that *there is no preference for mirror symmetry breaking during CNT deforming*. This is clearly seen for (7,7) and (8,8) CNTs whose gap results are shown in Figs. 5(a) and 5(b), respectively. In the course of deforming of these tubes, mirror symmetry is broken at $d_{\mathrm{TB}} \sim 3.4$ Å and a gap is formed around E_F. After 1–2 steps mirror symmetry is recovered and the gap closes at an early stage, as seen in the graphs of Figs. 5(a) and 5(b).

The major differences of the larger diameter nanotubes are (i) the initiation of the band gap at smaller deformation when mirror symmetry is broken, and (ii) the increased stability of the system in the course of deforming. This stability is due to robustness of the CNT conformation with respect to the tip: larger tubes have more atoms at the surface interacting with graphene layers. Hence "tank-treading" as well as translational motion is less significant. Therefore, we expect that *for CNTs with large diameters, the band-gap opening is more reproducible*.

D. Effect of self-consistency

All our calculations are based on DF-TB parameterization. However, such empirical potentials may suffer from transferability problems, especially for largely deformed structures. Hence we need to check the validity of our conclusions using better models. To test our results, we consider the calculations of (6,6) CNT structures displayed in Figs. 2(a), 2(b), and 2(d). Band-gap calculation using DF-TB model is compared to calculations within self-consistent density functional tight binding model (SCTB) (Refs. 12 and 13) and density functional theory calculations (DFT).[18] The latter is performed using GAUSSIAN03 framework[19] within BPW91 exchange-correlation functional parametrization[20] and 6-31G basis set.

In Fig. 6 we show the band-gap calculation results for the three different simulations using different models. When the CNT conserves its mirror symmetry a band-gap cannot develop at E_F. The three models agree and the results are identical as shown in Fig. 6(a). When mirror symmetry is broken, the three models predict a band-gap opening, *nonmonotonic behavior* and closure in the same region of deformation, but the magnitude depends strongly on the description of the interaction. In particular, DF-TB results which are shown as dotted lines with open circles in Fig. 6 do not incorporate charge redistribution. Such a description is reasonable for small deformation. However as d_{TB} decreases below 3.3 Å, charge can redistribute between carbon atoms and this may result in different electronic properties. The importance of charge transfer revealed in the SCTB calculations is shown as a continuous line in Fig. 6. It diverges from the DF-TB model only under strong deformation, $d_{\mathrm{TB}} < 3.3$ Å.

The band gap calculated within the DFT is different from the DF-TB model. The origin of this difference is *twofold*: DFT underestimates the band gap and DF-TB model fails to describe the long range interaction. When mirror symmetry is broken, both DF-TB and DFT predict mismatch between sublattices **A** and **B**, but the strength of the mismatch depends on the interaction. Within DFT parameterization, the exchange correlation functional is underestimated and hence

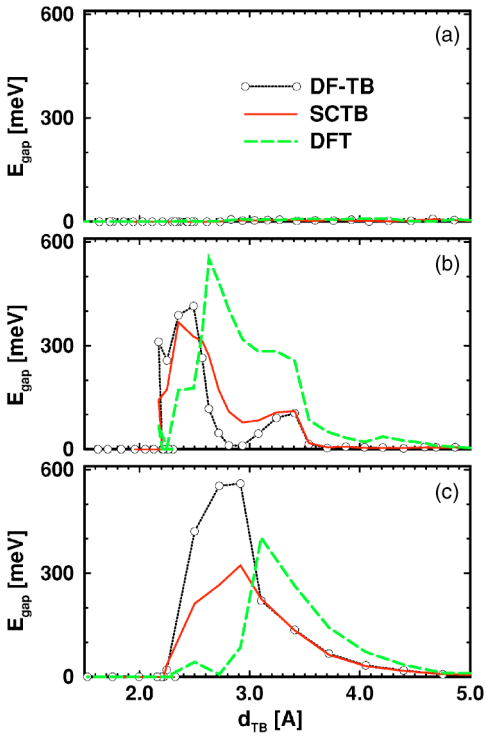


FIG. 6. (Color online) Energy gap of (6,6) CNT at E_F as a function of separation distance between top and bottom sides of CNT (d_{TB}) for simulations shown in Figs. 2(a), 2(b), and 2(d). Dotted lines with open circles are the original calculations within the DF-TB model. Solid and dashed lines correspond to calculations using SCTB and DFT, respectively.

the band gap is smaller than DF-TB results under large deformations. However, at $d_{\mathrm{TB}} \geqslant 3.5$ Å, DF-TB fails to describe long range interaction due to an imposed cut-off radius of 5.2 Å. This causes DFT results to be larger than those of DF-TB. Therefore, for large diameter deformed CNTs with broken mirror symmetry a band-gap can develop at much earlier stage, i.e., at $d_{\mathrm{TB}} > 5.0$ Å.

Finally we note that our results derived from the three models are in qualitative agreement, and our conclusion deduced from DF-TB calculations are valid. Quantitatively E_g depends on the model and some differences emerge. In particular, within DFT model conductance oscillations are less pronounced and disappear in Fig. 6(b). However, this model predicts E_g oscillations in Fig. 6(c) and the band gap vanishes $d_{\mathrm{TB}} \sim 2.8$ Å.

V. CONCLUSION

We have performed the state of the art DF-TB MD simulations of deforming armchair CNT. Our analyses have been carried out on tubes with diameters in the range of 8–16 Å. Such a large number of simulations enable to have more conclusive analysis on these systems and we find that:

(1) Force required to deform CNT increases with tube diameter and is larger for conformations with mirror symmetry preserved. The path for deforming an armchair CNT can be split into *three* different regimes. For $d_{\mathrm{TB}} > 3.8$ Å, the

force exerted on the AFM tip is small (<10 nN/per CNT unit cell) and the CNT undergoes most of the compression. In the intermediate regime, $d_{\mathrm{TB}} \sim 2.3$–3.8 Å, force is substantially enhanced and reaches 40–100 nN/per CNT unit cell. Finally, for $d_{\mathrm{TB}} < 2.3$ Å, CNT is under strong deformation. It undergoes atomic relaxation and looses its hexagonal shape, resulting in force drop-off.

(2) If CNT mirror symmetry is broken, E_g can develop due to mismatch between sublattices **A** and **B**. However, this distinguishability between the sublattices is due to top-bottom interactions as well as edge effects. The former can be modeled within single π-orbital/atom while the latter has a strong π–σ interaction and cannot be represented within the single π-orbital/atom.

(3) The band gap is initiated primarily due to the top-bottom interactions, but for $d_{\mathrm{TB}} \leqslant 3.5$ Å mismatch at the edges becomes important and can lead to cancellation of the band gap formed. This can result in band-gap oscillation as a function of deforming. However this effect depends on the exact atomic position at the edges. Hence we do not expect smooth variation of the conductance as a function of deforming.

(4) Under strong deformation CNT loses its honeycomb structure and becomes metallic.

(5) Large diameter CNTs have more contact area with AFM tip during deforming. Hence, their conformation with respect to the tip is more robust. Their deforming results are expected to be more reproducible in an AFM experiment performed in the reversible regime of the CNT structure.

(6) Band-gap formation of deformed armchair CNT described by DF-TB, SCTB, and DFT models are in qualitative agreement. However, quantitatively the value of the band gap is model dependent. Under large deformation, $d_{\mathrm{TB}} < 3.5$ Å, charge transfer is important and band gap is overestimated within the DF-TB model. In addition to this, the DF-TB model underestimates long range interaction. Hence interaction between top and bottom sides of the CNT are underestimated and this results in a smaller gap compared to DFT for $d_{\mathrm{TB}} > 3.5$ Å. Hence large diameter deformed CNTs with broken mirror symmetry, are expected to develop a band gap even for $d_{\mathrm{TB}} \geqslant 5.0$ Å.

ACKNOWLEDGMENTS

H.M. was supported by NASA Contract to UARC/ELORET and NSERC of Canada. A.S. and M.P.A. was supported by NASA contract to UARC. We are grateful to Dr. A. Maiti and Dr. J. Okeeffe for useful discussions.

[1] S. Paulson, M. R. Falvo, N. Snider, A. Helser, T. Hudson, A. Seeger, R. M. Taylor, R. Superfine, and S. Washburn, Appl. Phys. Lett. **75**, 2936 (1999).

[2] C. Gomez-Navarro, P. J. DePablo and J. Gomez-Herrero, Adv. Mater. (Weinheim, Ger.) **16**, 549 (2004).

[3] T. W. Tombler, C. Zhou, L. Alexseyev, J. Kong, H. Dai, L. Liu, C. S. Jayanthi, M. Tang, and S.-Y. Wu, Nature (London) **405**, 769 (2000)

[4] E. D. Minot, Y. Yaish, V. Sazonova, J-Y. Park, M. Brink, and P. L. McEuen, Phys. Rev. Lett. **90**, 156401 (2003).

[5] J. Cao, Q. Wang, and H. Dai, Phys. Rev. Lett. **90**, 157601 (2003).

[6] Yu. N. Gartstein, A. A. Zakhidov, and R. H. Baughman, Phys. Rev. Lett. **89**, 045503 (2002); Phys. Rev. B **68**, 115415 (2003).

[7] A. Maiti, A. Svizhenko, and M. P. Anantram, Phys. Rev. Lett. **88**, 126805 (2002); L. Yang, M. P. Anantram, J. Han, and J. P. Lu, Phys. Rev. B **60**, 13874 (1999); A. Heyd, A. Charlier, and E. McRae, *ibid.* **55**, 6820 (1997).

[8] Ç. Kılıç, S. Ciraci, O. Gülseren, and T. Yildirim, Phys. Rev. B **62**, R16345 (2000).

[9] C. J. Park, Y. H. Kim, and K. J. Chang, Phys. Rev. B **60**, 10656 (1999).

[10] O. Gülseren, T. Yildirim, S. Ciraci, and Ç. Kılıç, Phys. Rev. B **65**, 155410 (2002).

[11] J.-Q. Lu, J. Wu, W. Duan, F. Liu, B.-F. Zhu, and B.-L. Gu, Phys. Rev. Lett. **90**, 156601 (2003).

[12] M. Elstner, D. Porezag, G. Jungnickel, J. Elsner, M. Haugk, T. Frauenheim, S. Suhai, and G. Seifert, Phys. Rev. B **58**, 7260 (1998).

[13] T. Frauenheim, G. Seifert, M. Elstner, Z. Hajnal, G. Jungnickel, D. Porezag, S. Suhai, and R. Scholz, Phys. Status Solidi B **217**, 41 (2000).

[14] H. Hellmann, *Einfuhrung in die Quantum chemie* (Deuticke, Leipzig, 1937).

[15] R. P. Feynman, Phys. Rev. **56**, 340 (1939).

[16] Two carbon atoms define a graphene unit cell. Hence graphene can be viewed as a superposition of two sublattices each composed of a single atom. This defines sublattices **A** and **B** which have identical interactions for ideal CNT.

[17] To determine unit vector **U** corresponding to the π-direction at every carbon atom, we initially find the unit vectors $\mathbf{C}_1$, $\mathbf{C}_2$, and $\mathbf{C}_3$ in the direction of the three nearest neighbors of the carbon atom. Three vectors, $\mathbf{V}_1$, $\mathbf{V}_2$, and $\mathbf{V}_3$ are defined such that $\mathbf{V}_i = \epsilon_{ijk}(\mathbf{C}_i.\mathbf{C}_j)\mathbf{C}_k + \epsilon_{ikj}(\mathbf{C}_i.\mathbf{C}_k)\mathbf{C}_j$. **U** should be orthogonal to the three vectors, $\mathbf{V}_1$, $\mathbf{V}_2$, and $\mathbf{V}_3$; hence **U** is determined such that $[\mathbf{V}_1\mathbf{V}_2\mathbf{V}_3]$. **U** has negligible elements.

[18] P. Hohenberg and W. Kohn, Phys. Rev. **136**, B864 (1964). W. Kohn and L. J. Sham, Phys. Rev. **140**, A1133 (1965).

[19] GAUSSIAN 03 (Gaussian, Inc., Pittsburgh, Pennsylvania, 2003).

[20] K. Burke, J. P. Perdew, and Y. Wang, in *Electronic Density Functional Theory: Recent Progress and New Directions*, edited by J. F. Dobson, G. Vignale, and M. P. Das (Plenum, New York, 1998).